RADIO SCIENCE, VOL. 41, RS6005, doi:10.1029/2006RS003463, 2006

A model to predict cloud density from midlatitude atmospheric soundings for microwave radiative transfer applications

Nazzareno Pierdicca,[1] Luca Pulvirenti,[1] and Frank S. Marzano[1]

Received 16 January 2006; revised 16 June 2006; accepted 14 August 2006; published 15 December 2006.

[1] A new model for computing cloud liquid density from vertical profiles of meteorological variables, provided by either radio soundings or atmospheric analyses, is proposed. It has been developed for local-scale applications, in particular for a midlatitude environment such as the Mediterranean area, although the methodology can be easily extended to other climatic zones. The model has been derived from a numerical simulation of a cloudy event that occurred in the Mediterranean basin, performed by means of a microphysical mesoscale meteorological simulation package. The validation has been mainly carried out through a comparison between brightness temperature simulations in cloudy conditions and satellite microwave radiometric data over the Mediterranean Sea. The simulations have been performed by applying a radiative transfer scheme to a set of atmospheric profiles consisting of both European Centre for Medium-Range Weather Forecasts (ECMWF) analyses and radiosonde measurements. Two literature models have been considered as benchmarks. The new model reproduces the Special Sensor Microwave Imager brightness temperature statistics in the Mediterranean area fairly well. Furthermore, it predicts an integrated liquid water content which is in agreement with that supplied by the ECMWF analyses.

Citation: Pierdicca, N., L. Pulvirenti, and F. S. Marzano (2006), A model to predict cloud density from midlatitude atmospheric soundings for microwave radiative transfer applications, *Radio Sci.*, *41*, RS6005, doi:10.1029/2006RS003463.

1. Introduction

[2] An accurate evaluation of the attenuation produced by clouds and water vapor on the microwave signal propagating through the atmosphere represents a crucial aspect for communication and remote sensing studies [*Altshuler and Marr*, 1989; *Dintelmann and Ortgies*, 1989]. While much work has been done on water vapor absorption [e.g., *Liebe and Layton*, 1987; *Liebe et al.*, 1993; *Rosenkranz*, 1998], cloud attenuation remains a source of uncertainty [*Slobin*, 1982; *Löhnert and Crewell*, 2003]. This is mainly because of the lack of reliable information concerning cloud liquid, whereas vapor absorption amount can be based on data furnished by radiosonde observations (RAOBs) or atmospheric analyses, such as those provided by the European Centre for Medium-Range Weather Forecasts (ECMWF).

[3] Statistics of cloud attenuation have been computed by *Slobin* [1982] from meteorological data concerning various sites in the United States. Simple attenuation models have been developed by *Altshuler and Marr* [1989] and by *Dintelmann and Ortgies* [1989]. The former computes this parameter as a function of elevation angle, frequency, and air humidity at surface, while the latter predicts attenuation statistics from ground-based air humidity and temperature measurements. As noticed by *Salonen and Uppala* [1991], these two methods are based on data collected in one site only and cannot be trustfully applied in other climatic areas. *Chernykh and Eskridge* [1996] have used the minimum dew point depression and the corresponding temperature to estimate the cloud amount via the empirically derived *Arabey* [1975] diagram. Also in this case the validation was carried out by considering radiosondes launched from the United States only.

[4] The development of a model (hereinafter named cloud density model) to estimate cloud liquid density from vertical profiles of atmospheric variables is very important, not only for predicting attenuation in radio propagation problems, but also to apply radiative transfer schemes for simulating the radiance observed by a spaceborne radiometer. Radiometers operating in the microwave band are able to remotely retrieve long time series of geophysical variables useful for climatic studies

[1]Department of Electronic Engineering, University La Sapienza of Rome, Rome, Italy.

0048-6604/06/2006RS003463$11.00

[*Wentz*, 1997], and most of the retrieval methods are trained using brightness temperature (TB) simulations. In previous works [e.g., *Pierdicca et al.*, 2004; *Pulvirenti and Pierdicca*, 2006], we have demonstrated that, to increase the reliability of the synthetic TBs and, consequently, the accuracy of the retrieval, it is important to take into account the climatic characteristics of the geographical area of interest in the forward radiative model. As will be discussed later on, the use of two widely adopted cloud density models, such as those proposed by *Decker et al.* [1978] and by *Salonen and Uppala* [1991] (detailed in section 2), produces in the Mediterranean area simulated TBs which, in cloudy conditions, may show significant discrepancies with respect to actual measurements.

[5] The aim of this work is the improvement of the reliability of the TB simulations in cloudy conditions with respect to that achievable by applying commonly adopted literature methods. The study is focused on the Mediterranean area, which deserves the attention of a large community. The new cloud density model developed in this paper is based on the outputs of a numerical simulation of a cloudy event, derived from a mesoscale forecast system with explicit cloud microphysics [e.g., *d'Auria et al.*, 1998; *Marzano and Roberti*, 2003]. Being based on synthetic data, this procedure can be, in principle, applied to any geographical zone where mesoscale simulations are available. Following this idea, in this work we propose a new cloud density model valuable for a midlatitude climatology and in particular, to support propagation studies and microwave radiometry applications in the Mediterranean area. Moreover, we assess its impact on the TBs simulated by means of a radiative transfer scheme in comparison with what can be achieved by literature methods.

[6] The assessment of the accuracy of the considered cloud density models has been accomplished by implementing them within a plane-parallel radiative transfer algorithm. The corresponding simulations have been compared with the measurements of the Special Sensor Microwave Imager (SSM/I) above a sea background, since, over land, TBs are not very sensitive to cloud liquid [*d'Auria et al.*, 1998]. As inputs to the radiative transfer scheme, we have used the analyses provided by the ECMWF, as well as a set of radiosonde measurements of several Italian coastal stations collected throughout a long period of time. RAOBs represent the typical source of data to which atmospheric radiative models are applied for the purpose of obtaining both liquid water and gas absorption data, exploiting their good vertical resolution. On the other hand, ECMWF analyses supply also meteorological profiles above the sea surface, thus being particularly suitable for comparisons with radiometric measurements over such background [e.g., *Gerard and Eymard*, 1998]. Moreover, they furnish a value of integrated liquid water content which may give another term of comparison for assessing the various methods. It is worth reminding that neither RAOBs nor ECMWF analyses provide the profile of liquid density, which is required by radiative transfer to produce a synthetic TB, thus justifying the need for a cloud density model.

[7] The paper is organized as follows. Section 2 gives an overview of the considered literature models. In section 3, the procedure that we have followed to develop the new model is depicted in detail. Section 4 analyzes the results of the comparisons between simulated and measured brightness temperatures and between the various integrated liquid water contents.

2. Overview of Cloud Density Models

[8] Despite the mentioned difficulty to assess any method to compute cloud liquid water content (LWC) from vertical atmospheric profiles, several models have been developed in the last two decades for estimating LWC in each atmospheric layer. Among them, in this paper we have taken into consideration the algorithm proposed by *Decker et al.* [1978] (hereinafter the Decker model) and that developed by *Salonen and Uppala* [1991], updated by *Martellucci et al.* [2002] (hereinafter the Salonen model). They are widely used in radiative transfer algorithms [e.g., *Ware et al.*, 2003], as well as to predict cloud attenuation [*Marzano and Riva*, 2003; *Ventouras and Wrench*, 1999]. To obtain LWC in each layer, two steps are required. The first one consists of detecting the presence of a cloud from the relative humidity (RH) of each level, and it is usually based on the definition of a threshold, known as critical humidity (RH_c) [e.g., *Wang et al.*, 1999], although an alternative approach has been proposed, based on the second derivatives of both humidity and temperature [*Chernykh and Eskridge*, 1996]. The second step is represented by the actual computation of LWC.

[9] As for RH_c, it is generally accepted that it can be less than 100%. *Minnis et al.* [2005] have demonstrated that water clouds having the 90% of cloud cover may occur even when RH is around 70%, and *Zhang* [2003] has supposed that the existence of a significant amount of cloud for low RH may be due to the vertical resolution of the data (i.e., the cloud is thinner than the layer extension). The presence of cloud droplets in layers characterized by low RH may be also due to the vertical motion that is accounted for in a nonhydrostatic system. Since any misdetection of clouds can affect propagation computations even for fractional cloud amount less than 100%, the consideration of RH_c less than 100% becomes important.

[10] The Decker model assumes a constant value for the critical humidity. It is an adjustable parameter, and

we have chosen $RH_c = 0.95$, as proposed in the original paper [*Decker et al.*, 1978]. As for the computation of LWC, it supposes that the liquid density within a cloud is constant and proposes three simple relationships which relate LWC of nonprecipitating clouds, in g m^{-3}, to their thickness (τ), in km. The first relationship is represented by the following equations:

$$\mathrm{LWC} = 1.6\,\tau \tag{1a}$$

$$\mathrm{Max(LWC)} = 0.8\ \mathrm{g\ m^{-3}} \tag{1b}$$

$$\mathrm{Min(LWC)} = 0.2\ \mathrm{g\ m^{-3}}. \tag{1c}$$

Equations (1b)–(1c) impose that LWC cannot be less than 0.2 g m^{-3} and greater than 0.8 g m^3. The other two relationships are similar to equations (1a)–(1c), except for a multiplication factor equal either to 0.5, or to 0.25. In other words, Decker proposes three models relating liquid density to cloud thickness in order to account for the extreme variability of LWC. The analysis described in section 4 will consider only the third one (i.e., that characterized by the multiplication factor of 0.25), in order to limit the strong overestimation of simulated TBs in cloudy conditions obtained by applying the other factors.

[11] The approach followed by Salonen has been based on the ECMWF forecasting system. It supposes that RH_c depends on the ratio between the atmospheric pressure (P) within a cloud layer and the surface pressure (P_s), according to the following equation:

$$\mathrm{RH_c} = 1 - \sigma(1-\sigma)\left[1 + \sqrt{3}(\sigma - 0.5)\right], \tag{2}$$

where $\sigma = P/P_s$. LWC is a function of the altitude of the cloud layer above the cloud base in m (H_b) and of the air temperature in °C (T_c):

$$\mathrm{LWC} = \mathrm{LWC_0}(H_b/1500)(1 + 0.04T_c)Q(T_c), \tag{3}$$

where $\mathrm{LWC_0} = 0.14$ g m^{-3} and $\mathrm{Q}(T_c)$ is given by

$$\mathrm{Q}(T_c) = \begin{cases} 1 & T_c > 0^\circ\mathrm{C} \\ 1 + T_c/20 & -20^\circ\mathrm{C} < T_c \le 0^\circ\mathrm{C}. \\ 0 & T_c \le -20^\circ\mathrm{C} \end{cases} \tag{4}$$

Equations (3) and (4) have been developed using the statistics of cloud properties for different thicknesses and temperatures in the former Soviet Union. From such relationships it can be inferred that, for a height above the cloud base of 1500 m and for $T_c = 0$°C, LWC is equal to 0.14 g m^{-3}. Such value has been tuned to match attenuation distributions measured in Finland. In work by *Martellucci et al.* [2002], $\mathrm{LWC_0}$ has been slightly changed (0.17 g m^{-3}) and equation (3) has been modified, only for temperatures less than 0°C, as in the following:

$$\mathrm{LWC} = \mathrm{LWC_0}(H_b/1500)[\exp(0.04T_c)]\mathrm{Q}(T_c). \tag{5}$$

Hereafter, for the Salonen model we will include the update represented by equation (5).

3. Development of a Simulation-Based Cloud Density Model

[12] An assumption of a constant LWC within the cloud vertical extension, as in the Decker model, appears too simplistic. *Löhnert and Crewell* [2003] and *Löhnert et al.* [2004] have shown that the mean LWC vertical profile is too far to be constant. As for the Salonen method, it has been tuned to climatic conditions which are different from those characteristic of a midlatitude climatic area. We have therefore tried to derive a new model starting from a simulation experiment carried out by means of the Advanced Regional Prediction System (ARPS).

[13] ARPS is a nonhydrostatic mesoscale numerical model that has shown good accuracy in predicting cloudy events occurring at the Mediterranean latitudes [*Souto et al.*, 2003]. With respect to general circulation models, such as the ECMWF system, its detailed microphysical characterization makes it suitable for radiative transfer applications. The ARPS governing equations include conservation of momentum, heat, mass, water substances (water vapor, cloud water, rain, cloud ice, snow, and graupel), subgrid-scale turbulent kinetic energy, and the equation of state of moist air. These equations are represented in a curvilinear coordinate system, which is orthogonal in the horizontal. The modified three-category ice scheme of *Lin et al.* [1983] is used for microphysics parameterization. It contains two liquid phases (cloud and rain) and three ice categories (cloud ice, snow, and graupel). LWC is determined by solving the conservation equation for water species. In this equation, the source terms account for several processes such as condensation, evaporation of droplets, freezing of raindrops, melting of snow and graupel, deposition of ice particles, and sublimation of the latter. Furthermore, the microphysical transfer rates between the hydrometeor species pairs are considered. To provide detailed initial conditions, ARPS has a sophisticated data analysis system (named ADAS: ARPS Data Analysis System) which includes a three-dimensional cloud analysis package. Further details on ARPS can be found in work by *Xue et al.* [2000, 2001].

3.1. Mesoscale Cloud Model Data Analysis

[14] ARPS has been run to simulate a cloudy event that occurred in the Mediterranean basin on 3–4 November 2000. Such an event was characterized by low stratiform clouds, producing either no rain or moderate rain. The realism of the simulated cloud locations has been verified by means of corresponding METEOSAT images. Moreover, for the situations in which precipitation was present, we have compared the rain rate, predicted by ARPS, with rain gauge data available from a network situated in central Italy (close to the Tyrrhenian coast), and we have found a fairly good matching. ARPS simulations of this event can be therefore considered very realistic. The outputs of the simulation, spanning a time period of 36 hours, consist of the following variables: cloud, rain, graupel, ice, and aggregate densities (g m^{-3}), relative and specific humidity, pressure, and temperature. Such variables are furnished each hour (i.e., 36 outputs have been produced) on a geographical grid of 110 by 110 pixels whose limits are 38.4°–46.3°N, 6.6°–17.4°E. The vertical resolution is 500 m, except for the first level, which is 250 m above the sea level. The number of layers is 33. The choice of a midseason event has been done to avoid considering extreme meteorological conditions, thus ensuring compatibility with several situations occurring in the Mediterranean area. Moreover, the selected event is fairly long, thus permitting us to acquire a large number of cloud samples.

[15] The mesoscale model simulation has been used as a physically based random generator of cloud profiles in a variety of thermodynamic and dynamical conditions. From this point of view, the representativeness of a single simulation may be regarded as a critical aspect. Nevertheless, it originates a cloud density model performing better than the literature ones in the Mediterranean area, as will be proved hereafter. Even though the availability of additional simulations may be problematic, the methodology we propose can be further exploited and extended by considering different mesoscale forecast model runs, associated to various stratiform events in the specific climatological context.

[16] While ARPS includes complex relationships describing the microphysics of the cloud formation, our aim is to obtain a simple estimator of RH_c and LWC from atmospheric vertical profiles measured by radiosondes or supplied by ECMWF. Standard regression analysis has been applied for this purpose. We have first identified each of the 36 outputs of the ARPS run by an index (from 1 to 36), and those having an odd index have been used to estimate the relationships to compute RH_c and LWC, while the others have been utilized to test its validity. In the following, the profiles associated with an odd index will be denoted as training profiles, whereas the even will be denoted as test ones. In order to design the optimal regression algorithm (i.e., number of predictors and functional form), only the relative changes of regression accuracy are of interest, and the correlation between the forecasts at successive time steps (i.e., between training and test profiles) is not crucial. We have chosen a LWC threshold equal to 10^{-3} g m^{-3} to recognize the presence of a cloud in each layer, thus assuming that only LWCs $> 10^{-3}$ g m^{-3} produce a detectable effect on the TB measured by a satellite radiometer. Moreover, only those profiles characterized by at least two layers with LWC $> 10^{-3}$ g m^{-3} and by absence of surface rain rate have been considered. In this way, we have retained about 190,000 vertical profiles among the 435,600 ($110 \times 110 \times 36$) ones generated by ARPS.

3.2. Cloud Density Model Development

[17] To determine the critical relative humidity, for each layer of the ARPS profiles we have derived the histogram of RH in the presence of clouds, and we have computed RH_c as the threshold value above which 95% of the whole histogram area occurs. We have paid attention to exclude some isolated peaks in the histograms relative to high layers (probably due the vertical motion of cloud droplets that is accounted for in a nonhydrostatic system) which, if considered, would have caused unreasonably low RH_c values. Assuming that, as in the Salonen model, for a given level, RH_c mainly depends on the ratio P/P_s (still denoted by σ), we have calculated the mean value of σ for each layer in which LWC $> 10^{-3}$ g m^{-3}. Finally, for the training profiles, we have accomplished a polynomial fitting of the relationship $RH_c - \sigma$. We have found that the following third-degree polynomial best fits such a relationship:

$$RH_c = \begin{cases} 3.04394 - 9.97858\sigma + 13.7378\sigma^2 \\ \quad -5.86410\sigma^3 & 0.344 \le \sigma \le 1 \\ 1 & \sigma < 0.344 \end{cases}. \tag{6}$$

It is worth noticing that it has been imposed that RH_c cannot be greater than 1.

[18] Figure 1 shows the plot of the critical humidity versus the mean value of the ratio P/P_s for the ARPS test profiles (asterisks). The relationships between RH_c and σ, computed by applying equation (6) (dashed line), the Salonen model (i.e., equation (2), dash-dotted line), and the Decker one (i.e., a vertical dotted line representing the equation $RH_c = 0.95$) are also shown. By observing Figure 1, it can be inferred that through the application of equation (2) to the ARPS test vertical profiles, there are several false alarm situations in which a cloud is detected, but it is not actually present in a given ARPS layer. Conversely, a threshold equal to 95% seems to

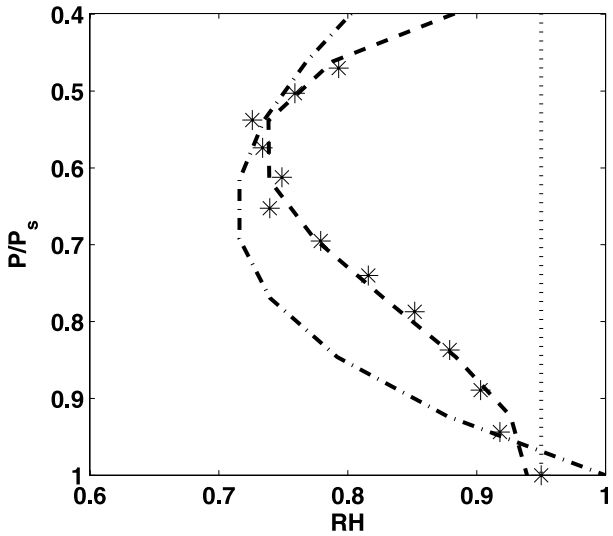

Figure 1. Critical relative humidity versus mean value of the ratio between atmospheric pressure and surface pressure for each layer of the ARPS test profiles (asterisks). The critical humidity as function of the normalized air pressure computed by the new model (dashed line), the Salonen method (dash-dotted line), and the Decker one (dotted line) are also shown.

be too conservative, giving rise to situations of missed detection of a cloud; that is, the model does not reveal a cloud when it is actually present. Table 1 reports the percentages of correct and wrong detections obtained by applying the three different equations for RH_c to the ARPS test profiles. The first two columns regard situations of clear sky (first column, correctly detected; second column, false alarm) and their sum is equal to 1 for each row. The other two columns concern cloudy situations (third column, cloud correctly revealed; fourth column, missed detection). Also in this case, their sum is equal to 1 for each row. The fairly high probability of false alarm due to the application of equation (2) is confirmed (20%), whereas a critical humidity equal to 0.95 tends to annul false alarms but to excessively increase missed detection (12%). Equation (6) seems to be an acceptable tradeoff between these two situations.

[19] As for the computation of cloud liquid density, we have adopted a regression approach in which, as predictors, we have selected H_b (height above cloud base in m) and T_c (temperature in °C). It is worth noticing that the same predictors used in the Salonen model are considered. This is not surprising, since the goal of any semiempirical cloud density model is to estimate LWC from the available temperature, pressure, and relative humidity data at a given height. Including other variables in the regression, such as pressure or vapor density, has been demonstrated not profitable to improve the regression accuracy. We have selected only those samples belonging to the training set characterized by LWC $> 10^{-3}$ g m^{-3} and by $T_c \geq 0$°C, and we have performed a regression analysis by assuming a functional form relating LWC to our predictors of the type depicted in equation (7a), which is the one that provides the best fitting performances. By analyzing our training profiles, we have found that LWC tends to exponentially decay with the decrease of temperature when the latter is less than 0°C and that a simple multiplication of equation (7a) for a factor equal to $\exp(0.176565T_c)$ allows estimating LWC also for these cases. To ensure the physical consistency of our new model, we have excluded the presence of cloud liquid for $T_c < -30$°C. Furthermore, we have imposed that once $RH \geq RH_c$, the minimum liquid density cannot be less than the threshold. In conclusion, the model we propose has the following form:

$$\mathrm{LWC} = \begin{cases} a_0 + a_1 H_b + a_2 (H_b T_c) & T_c > 0^\circ\mathrm{C} \quad (7a) \\ [a_0 + a_1 H_b + a_2 (H_b T_c)] \exp(0.176565 T_c) & -30^\circ\mathrm{C} < T_c \leq 0^\circ\mathrm{C} \quad (7b) \\ 0 & T_c \leq -30^\circ\mathrm{C} \quad (7c) \end{cases}$$

$$\mathrm{Min(LWC)} = 10^{-3}\ \mathrm{g\ m^{-3}}, \quad (7d)$$

where H_b is obviously always greater than 0. The coefficients a_0, a_1, and a_2 of equations (7a)–(7b) are 0.0216309, 0.00013736224, and 1.2552634×10^{-5}, respectively. Such an exercise can be carried out also for different geographical zones, if numerical simulations supplied by mesoscale nonhydrostatic forecast models are available.

[20] Table 2 reports the results of the application of equations (7a)–(7d) to the ARPS test profiles compared to the original ARPS LWC in terms of correlation

Table 1. Percentages of Correct and Wrong Detections of Both Cloud and Clear Sky Occurrences Obtained by Applying the Three Cloud Density Models to the ARPS Test Profiles[a]

	Clear Sky		Cloudy Situations	
	Correctly Detected	False Alarm	Correctly Detected	Missed Detection
Decker model	0.93	0.07	0.88	0.12
Salonen model	0.80	0.20	0.97	0.03
New model	0.87	0.13	0.95	0.05

[a]The sum of the first two columns of each row (concerning clear sky situations), as well as that relative to the third and the fourth ones (concerning cloudy situations), is 1.

Table 2. Statistical Analysis of the Results Obtained by Applying the Different Cloud Density Models to the ARPS Test Profiles, in Terms of Correlation Between ARPS and Estimated Liquid Water Contents and Root Mean Square (RMS) Error[a]

	Correlation Coefficient	RMS Error, g m^{-3}
Decker model	-	0.110
Salonen model	0.55	0.097
New model	0.70	0.082

[a]The correlation coefficient between ARPS and Decker LWCs is omitted, since it is not significant, being the Decker LWC constant for cloud thickness greater than only 500 m.

coefficient and root mean square (RMS) error. Table 3 shows the analogous data for the liquid water path (LWP), i.e., the LWC integrated over the cloud vertical extension. Tables 2 and 3 include the results obtained by adopting both the Decker and the Salonen models, except for the correlation coefficient between ARPS and Decker LWCs, which is not significant, being the Decker LWC constant for a cloud thickness greater than 500 m. A correlation between estimated and ARPS LWC of 0.70, as well as a fairly low RMS error, have been found for the new model. Also for LWP, the results seem to be encouraging and to improve those of the literature models. Our new estimator permits us to cover a good range of ARPS liquid densities, although we have verified that it tends to saturate for high LWCs (greater than 0.4 g m^{-3}). Such saturation is however less than that produced by the Salonen model.

[21] Figure 2 shows, for the test set, the mean LWC profile forecasted by ARPS (solid line), together with that estimated by our new model (dashed line) and by the Salonen one (dotted line). It emerges that the new model tends to follow the mean variability of ARPS profiles with altitude, especially below 1500 m. It presents a small overestimation of LWC between 1500 and 3500 m. Conversely, for high altitudes it tends to underestimate LWC. The improvement with respect to the Salonen model is, however, evident. With respect to the latter, our new cloud density model presents a different behavior, although both have the same predictors.

[22] Indeed, because it originated from ARPS simulations, the new model was expected to better reproduce the ARPS LWC forecasts. Consequently, we have accomplished an independent test of the various methods by comparing the synthetic TBs, derived from the three different cloud density models, to real radiometric observations.

Table 3. Statistical Analysis of the Results Obtained by Applying the Different Cloud Density Models to the ARPS Test Profiles in Terms of Correlation Between ARPS and Estimated Liquid Water Paths [cm] and Root Mean Square (RMS) Error

	Correlation Coefficient	RMS Error, cm
Decker model	0.64	0.035
Salonen model	0.75	0.026
New model	0.80	0.018

4. Application of the Models to Real Atmospheric Profiles

[23] In this section we focus on radiative transfer applications, in particular on the impact of the considered cloud density models on TB simulations. Such simulations have been generated by including each model in a plane parallel radiative transfer scheme, which uses the gas absorption proposed by *Liebe et al.* [1993]. It also adopts the Rayleigh approximation of the Mie scattering theory, thus assuming the absence of precipitation (i.e., presence of only small cloud droplets). The simulations concern the SSM/I instrument, which operates at 19.35, 37.0, and 85.5 GHz in both linear polarizations and at 22.2 GHz in vertical polarization. Here, we consider only the 19 and 37 GHz channels, because the 85 GHz ones are too sensitive to atmospheric scattering, while the 22 GHz synthetic TBs may be excessively influenced by the selected water vapor absorption model. We have taken into consideration only a "cold" marine background since, over land, the contribution of the cloud droplets to the observed brightness temperature makes it difficult to distinguish from that due to the underlying surface.

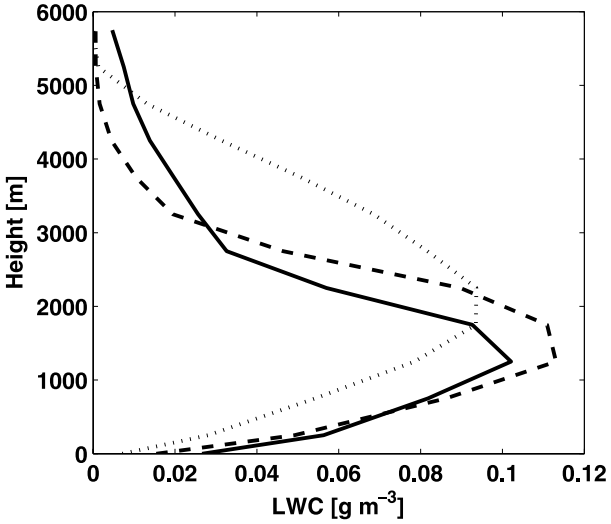

Figure 2. Mean cloud liquid density profile of the considered ARPS simulation (solid line) together with those estimated by the new model (dashed line) and by the Salonen one (dotted line).

[24] As a preliminary step, we have evaluated the impact on simulated TBs of the regressive model errors. By running the radiative transfer algorithm using alternatively the original ARPS mean profile and the mean profile predicted by our model (see Figure 2), a difference of about 0.54 K has emerged at 19 GHz (assuming a surface emissivity equal to 0.5).

[25] It has been already pointed out that although cloud density models are generally applied to RAOBs, ECMWF analyses can be exploited for performing a validation exercise, since they furnish atmospheric profiles over sea as well as a value of integrated liquid content. Consequently, we have initially used, as inputs to the radiative transfer calculations, the ECMWF analyses concerning grid points (0.5° resolution both in latitude and in longitude) in the Mediterranean Sea. The first 10 days of each month of year 2000 have been considered, and a set of SSM/I images regarding such period of time and the same geographical area have been collected for comparison. It must be taken into account that even a short temporal mismatch between ECMWF data and SSM/I observations at the same location may produce considerable differences between actual and synthetic ECMWF-derived TBs because of the quick evolution of the cloud cover. This makes unreliable a pixel-by-pixel comparison of colocated maps of liquid content. For this reason, the comparison has been based on the statistics of simulated and actual TBs; that is, it has been accomplished by comparing their histograms. The same statistical approach has been applied to the radiosonde-derived simulations.

[26] In order to perform a preliminary data screening (i.e., selection of cloudy data without precipitation, as described later), the ECMWF and SSM/I data sets have been colocated assuming a maximum distance between an ECMWF grid point and a SSM/I pixel equal to 15 km and a maximum time shift equal to 90 min. Through this procedure, we have built a database whose records contain the multifrequency and multipolarization synthetic TBs (19 and 37 GHz, both linear polarizations) produced by applying the three-cloud density models to each ECMWF atmospheric vertical profile, the corresponding three LWPs, the colocated actual TBs, and the values of LWP included in every analysis and those estimated by SSM/I. As LWP estimator from SSM/I data, we have chosen the algorithm proposed by *Gerard and Eymard* [1998].

4.1. Comparison of Liquid Water Path Estimates

[27] Figure 3 shows the results of a binned analysis of the RMS difference between LWPs computed by cloud density models and those supplied by ECMWF analyses. We have grouped LWP samples within intervals whose amplitude is 0.01 cm, and for each interval we have computed such RMS difference. For clarity, Figure 3 does not include the Decker method, which gives the worst results, as well as ECMWF LWP values lower than 0.1 cm. It can be noticed that for most of the intervals, our estimator presents the least RMS difference (especially for higher LWPs). Moreover, we have found that by applying our new model, a fairly high correlation coefficient (equal to 0.71) between ECMWF and computed LWPs is achieved, whereas with literature methods this parameter assumes lower values.

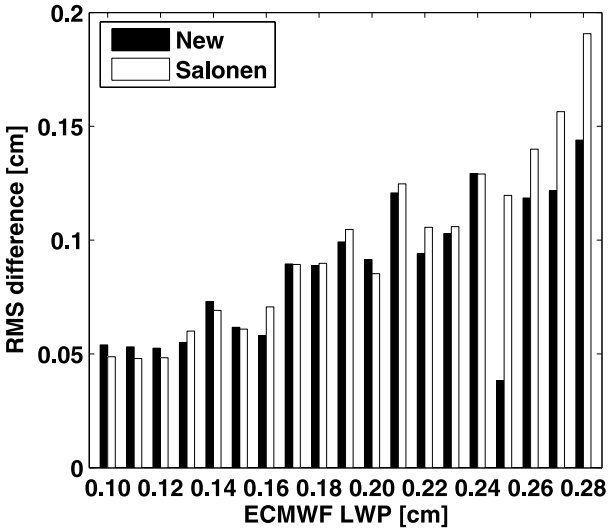

Figure 3. Binned analysis of the RMS difference between ECMWF liquid water path and those computed by applying the new model (black) and the Salonen one (white). Only ECMWF LWP values greater than 0.1 cm are considered. Data concern the Mediterranean Sea and the first 10 days of each month of year 2000.

[28] It must be underlined that because the ECMWF analyses are derived from a numerical model (for which LWC, which originates LWP, is a prognostic variable), we have not made a definitive validation of our approach. We have only verified that the new model is consistent not only with a single-event simulation carried out by means of ARPS, but also with the characteristics of the cloudy events in the same area throughout an entire year, foreseen by a different meteorological system operationally adopted for weather forecasts. This can be considered an indication that the dependency on the ARPS scheme is not a crucial problem. From this point of view, the comparison with the performances of the Salonen model shown in Figure 3 is encouraging since the latter is derived from ECMWF itself.

4.2. Comparison of Satellite Microwave Radiometric Features

[29] As far as the brightness temperature simulations are concerned, the whole forward model has been

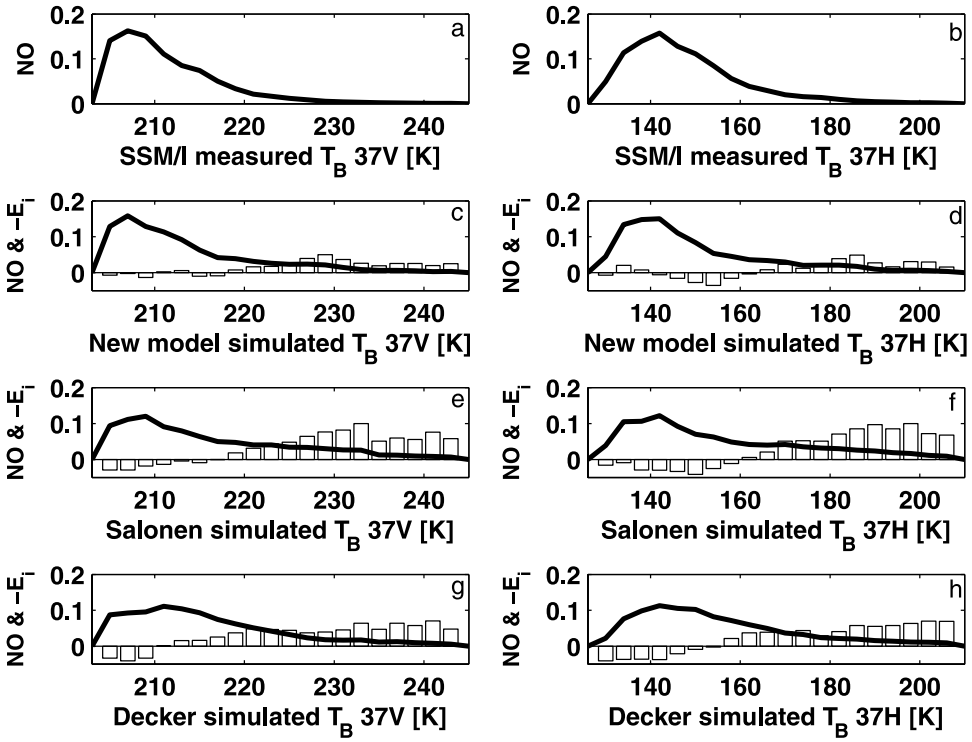

Figure 4. Comparison between the histograms (normalized occurrences, *NO*) of (a and b) SSM/I observations and those regarding the synthetic TBs obtained from (c and d) our new method and from (e and f) the Salonen and the (g and h) Decker ones. They concern the 37 GHz channels (left plots, vertical polarization; right plots, horizontal polarization). Simulations have been produced by applying a radiative transfer scheme, including the considered cloud density estimators, to ECMWF profiles. Figures 4c–4h show also the standardized residuals defined by equation (9). A negative scaling factor has been used for E_i to adopt the same vertical scale.

already validated in clear-sky conditions and for a sea background by means of a pixel-by-pixel comparison [*Pulvirenti and Pierdicca*, 2006]. This guarantees that the electromagnetic characterization of the sea surface emission and scattering, as well as of the absorption from the humid atmosphere, is fairly reliable. In cloudy conditions, the same kind of comparison is unreliable, so we have analyzed the results furnished by the various cloud density models in terms of simulated TBs by comparing their histograms with those derived from SSM/I measurements. Because the cloud density estimators are suitable for nonraining clouds, we have excluded records of the validation database characterized by a high probability of precipitation. For this purpose, we have used the scattering index (SI) proposed by *Ferraro and Marks* [1995], and we have retained only nonrainy samples of the validation database according to SSM/I (maximum SI equal to 5 K). In order to be reasonably sure to consider only cloudy situations, we have included only samples of the database characterized by both ECMWF and SSM/I detecting a cloud (the latter detection has been carried out by applying the algorithm developed by *Gerard and Eymard* [1998], as previously mentioned) and by at least two of the three cloud density models giving LWP > 0 cm. After these checks we have retained about 47,000 records.

[30] Figure 4 shows the comparison between the histograms of SSM/I observations (Figures 4a and 4b) and those regarding the synthetic TBs obtained from our new method (Figures 4c and 4d) and from the Salonen (Figures 4e and 4f) and the Decker (Figures 4g and 4h) ones. They concern the 37 GHz channels (left plots, vertical polarization; right plots, horizontal polarization), since they present the most significant discrepancies between simulated and actual data. Figure 4 shows the normalized occurrences *NO*, i.e., the number of TB measurements and simulations falling in a specified interval (of N_{bin} = 20 intervals, or bins, in which we have divided the range of brightness temperatures) normalized to the number N of SSM/I samples or M of simulation samples, respectively (in this case, $N = M \sim 47{,}000$, having colocated SSM/I and ECMWF pixels).

Table 4. Parameter C (Cramer's Phi) for the TB Simulations Produced by Applying to the ECMWF Profiles a Radiative Transfer Scheme Using the Three Cloud Density Predictors

	37 H, K	37 V, K	19 H, K	19 V, K
Decker model	0.23	0.29	0.12	0.12
Salonen model	0.25	0.29	0.12	0.12
New model	0.14	0.16	0.06	0.11

[31] It can be noticed that the histograms of TBs obtained using our cloud density model better reproduce those derived by the SSM/I measurements. In order to quantify this, we have performed a chi-square test of homogeneity [*Sheskin*, 2004], assessing whether two samples belong to the same population. The test is presented through the so-called Cramer's Phi parameter C, which is defined as the square root of the chi-square value χ^2 divided by the total number of samples:

$$\chi^2 = NM \sum_{i}^{N_{bin}} \frac{(X(i)/N - Y(i)/M)^2}{X(i) + Y(i)} \tag{8a}$$

$$C = \sqrt{\frac{\chi^2}{N+M}}, \tag{8b}$$

where $X(i)$ and $Y(i)$ denote the number of occurrences of measurements and simulations, respectively, within the ith bin. Table 4 reports the values of C derived using the three LWC models. It confirms that the samples of TBs originated from our cloud density model more likely belong to the same population of the measured ones, since the corresponding C is the lowest for all the considered channels (ideally, $C = 0$, i.e., identical statistical distributions). It is worth mentioning that we have also computed the mean values of the SSM/I TBs and of the synthetic ones for all the considered channels (not reported for the sake of concision), and we have found that they are more similar if our cloud density model is used.

[32] To analyze the behavior of the various methods for different TB ranges, we have considered the chi-square test for goodness of fit [*Sheskin*, 2004], which allows one to verify whether a distribution of samples is similar to a preordered one. In our case we have to test the distribution of simulated TBs against the measured one. The standardized residuals E_i have been computed for each bin:

$$E_i = \frac{[X(i) - Y(i)]}{\sqrt{X(i)}}. \tag{9}$$

These residuals have been superimposed on the histograms shown in Figure 4. Most of the real TBs are encompassed between 205 and 220 K (Figure 4a, vertical polarization) and between 130 and 160 K (Figure 4b, horizontal polarization). While the histograms relative to our new estimator seem to reproduce this characteristic, especially at vertical polarization (Figure 4c) for which the error bars are almost zero, those concerning literature methods appear too flat. Consequently, the latter predict a number of occurrences of high TBs (corresponding to high liquid densities) that is greater than that exhibited by SSM/I. This is corroborated by the observation of the E_is for the higher TBs. It can be noticed that our new liquid density estimator presents very short error bars if compared to those corresponding to the other predictors, except for a pair of bins at horizontal polarization (between 150 and 154 K).

[33] We have performed a further assessment by comparing the SSM/I data with those obtained by applying the three considered cloud density models to a set of radio-sounding observations (RAOBs) collected throughout years 1994–2002 from four Italian coastal stations. RAOBs present a better vertical resolution with respect to ECMWF analyses (up to 50 vertical layers instead of 17). However, some discrepancies between simulations and radiometric data must be expected not only because of the different acquisition times and locations, but also because of the different meteorological conditions (e.g., surface temperature, wind speed, and humidity) characterizing a costal environment with respect to the open sea. Nevertheless, this comparison can also give an indication of the capability of the models to estimate cloud liquid. As for the SSM/I data, here we consider the records, belonging to the database previously described, for which both ECMWF and SSM/I detect cloud (e.g., LWP > 0 cm) and characterized by SI < 5 K. As for the TB simulations derived from RAOBs profiles, we have considered samples for which at least two cloud density models predict LWP > 0 cm, thus considering about 11,000 records. With respect to the previous case, here $N \neq M$. Table 5 reports the Cramer's Phi parameter C, defined by equation (8), for this case. The new method provides again the best performances for every channel.

Table 5. Parameter C (Cramer's Phi) for the TB Simulations Produced by Applying to the RAOB Profiles a Radiative Transfer Scheme Using the Three Cloud Density Predictors

	37 H, K	37 V, K	19 H, K	19 V, K
Decker model	0.21	0.30	0.09	0.10
Salonen model	0.20	0.28	0.09	0.10
New model	0.10	0.18	0.05	0.07

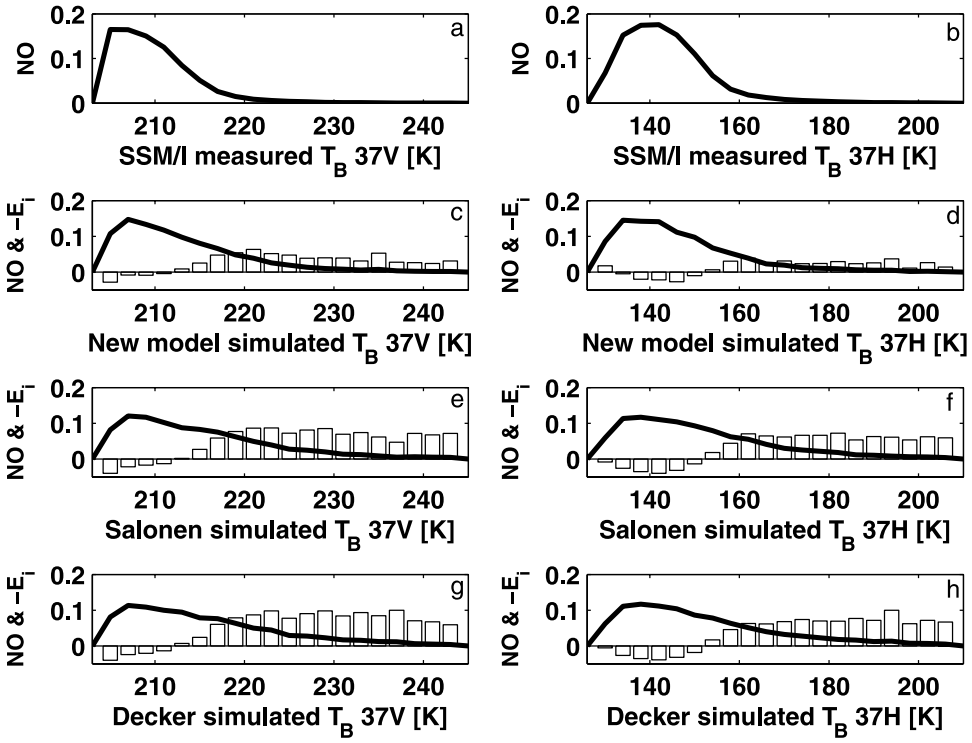

Figure 5. Comparison between the histograms (normalized occurrences, *NO*) of (a and b) SSM/I observations and those regarding the synthetic TBs obtained from (c and d) our new method and from (e and f) the Salonen and the (g and h) Decker ones. They concern the 37 GHz channels (left plots, vertical polarization; right plots, horizontal polarization). Simulations have been produced by applying a radiative transfer scheme, including the considered cloud density estimators, to RAOB profiles. Figures 5c–5h show also the error parameter E_i defined by equation (9). A negative scaling factor has been used for E_i to adopt the same vertical scale.

Figure 5 shows the various histograms together with the parameter E_i of equation (9) for the 37 GHz channels (analogous to Figure 4). It is confirmed that the application of the literature methods causes an excessive flattening of the histograms with respect to the SSM/I ones and overestimates the occurrence of higher values of TB. Also in this case, the E_i values associated with the new model are almost always the shortest in both polarizations (except the first bin at 37 H).

5. Conclusions

[34] A new simulation-based model to estimate cloud liquid density from an atmospheric vertical profile has been proposed for the purpose of improving the accuracy of brightness temperatures or attenuation simulations. It has been conceived for a midlatitude area, in particular for the Mediterranean basin, but the methodology can be easily extended to other climatic regions. We have used the outputs of a simulation of a stratiform cloudy event that occurred in the Mediterranean area. Such simulation has been carried out by using a microphysical mesoscale model named ARPS. Being developed for microwave radiative transfer applications, the method has been verified by evaluating its impact on satellite brightness temperature simulations. For this purpose we have included it in a radiative transfer scheme for a non-scattering atmosphere.

[35] Two literature models have been also considered as benchmarks. The application of the new method allows generating simulated TBs, originating from ECMWF analyses and radiosonde measurements, whose histograms are fairly able to reproduce those derived from the SSM/I data acquired in the Mediterranean area. This has been quantitatively shown using chi-square statistical tests. A comparison between liquid water paths given by ECMWF and computed by the new model has also revealed an improved matching. A strategy based on the use of a simulation produced by a mesoscale system therefore seems to be suitable to develop a simple estimator of cloud liquid. Future work will concern the possible improvement of the estimator by increasing the

number of numerical simulations, thus including different kinds of cloudy events and seasonal conditions.

[36] **Acknowledgments.** The authors would like to thank Slobodan Nickovic and his team at the University of Malta for running the ARPS model. They are also grateful to the reviewers for their profitable suggestions and comments.

References

Altshuler, E. E., and R. A. Marr (1989), Cloud attenuation at millimeter wavelengths, *IEEE Trans. Antennas Propag.*, *37*, 1473–1479.

Arabey, E. N. (1975), Radiosonde data as means for revealing cloud layers, *Meteorol. Gidrol.*, *6*, 32–37.

Chernykh, I. V., and R. E. Eskridge (1996), Determination of cloud amount and level from radiosonde soundings, *J. Appl. Meteorol.*, *35*, 1362–1369.

d'Auria, G., F. S. Marzano, N. Pierdicca, R. Pinna Nossai, P. Basili, and P. Ciotti (1998), Remotely sensing cloud properties from microwave radiometric observations by using a modeled cloud database, *Radio Sci.*, *33*, 369–392.

Decker, M. T., E. R. Westwater, and F. O. Guiraud (1978), Experimental evaluation of ground-based microwave radiometric sensing of atmospheric temperature and water vapor profiles, *J. Appl. Meteorol.*, *17*, 1788–1795.

Dintelmann, F., and G. Ortgies (1989), Semi-empirical model for cloud attenuation prediction, *Electron Lett.*, *25*, 1487–1488.

Ferraro, R. R., and G. F. Marks (1995), The development of SSM/I rain-rate retrieval algorithms using ground-based radar measurements, *J. Atmos. Oceanic Technol.*, *12*, 755–772.

Gerard, E., and L. Eymard (1998), Remote sensing of integrated cloud liquid water: Development of algorithms and quality control, *Radio Sci.*, *33*, 433–447.

Liebe, H. J., and D. H. Layton (1987), Millimeter wave properties of the atmosphere: Laboratory studies and propagation modeling, *NTIA Rep. 87-24*, 74 pp., Natl. Telecommun. and Inf. Admin., Washington, D. C.

Liebe, H. J., G. A. Hufford, and M. G. Cotton (1993), Propagation modeling of moist air and suspended water/ice particles at frequencies below 1000 GHz, *AGARD Conf. Proc.*, *542*, 3.1–3.10.

Lin, Y.-L., R. D. Farley, and H. D. Orville (1983), Bulk parameterization of the snow field in a cloud model, *J. Clim. Appl. Meteorol.*, *22*, 1065–1092.

Löhnert, U., and S. Crewell (2003), Accuracy of cloud liquid water path from ground-based microwave radiometry 1. Dependency on cloud model statistics, *Radio Sci.*, *38*(3), 8041, doi:10.1029/2002RS002654.

Löhnert, U., S. Crewell, and C. Simmer (2004), An integrated approach towards retrieving physically consistent profiles of temperature, humidity, and cloud liquid water, *J. Appl. Meteorol.*, *43*, 1295–1307.

Martellucci, A., J. P. V. Poiares Baptista, and G. Blarzino (2002), New climatological databases for ice depolarisation on satellite radio links, paper presented at COST 280 1st International Workshop, Eur. Coop. in the Field of Sci. and Technol., Malvern, U. K.

Marzano, F. S., and C. Riva (2003), Cloud-induced effects on monthly averaged scintillation amplitude along millimeter-wave slant paths, *IEEE Trans. Antennas. Propag.*, *51*, 880–887.

Marzano, F. S., and L. Roberti (2003), Numerical investigation of intense rainfall effects on coherent and incoherent slant-path propagation at K band and above, *IEEE Trans. Antennas Propag.*, *41*, 965–977.

Minnis, P., Y. Yi, J. Huang, and K. Ayers (2005), Relationships between radiosonde and RUC-2 meteorological conditions and cloud occurrence determined from ARM data, *J. Geophys. Res.*, *110*, D23204, doi:10.1029/2005JD006005.

Pierdicca, N., L. Pulvirenti, F. S. Marzano, P. Ciotti, P. Basili, and G. d'Auria (2004), Intercomparison of inversion algorithms to retrieve rain rate from SSM/I by using an extended validation set over the Mediterranean area, *IEEE Trans. Geosci. Remote Sens.*, *42*, 2226–2239.

Pulvirenti, L., and N. Pierdicca (2006), Retrieval of atmospheric and surface parameters from satellite microwave radiometers over the Mediterranean Sea, *IEEE Trans. Geosci. Remote Sens.*, *44*, 90–101.

Rosenkranz, P. W. (1998), Water vapor microwave continuum absorption: A comparison of measurements and models, *Radio Sci.*, *33*, 919–928.

Salonen, E., and S. Uppala (1991), New prediction method of cloud attenuation, *Electron. Lett.*, *27*, 1106–1108.

Sheskin, D. J. (2004), *Handbook of Parametric and Nonparametric Statistical Procedures*, 3rd ed., CRC Press, Boca Raton, Fla.

Slobin, S. D. (1982), Microwave noise temperature and attenuation of clouds: Statistics of these effects at various sites in the United States, Alaska and Hawaii, *Radio. Sci.*, *17*, 1443–1454.

Souto, M. J., C. F. Balseiro, V. Pérez-Muñuzuri, M. Xue, and K. Brewster (2003), Impact of cloud analysis on numerical weather prediction in the Galician region of Spain, *J. Appl. Meteorol.*, *42*, 129–140.

Ventouras, S., and C. L. Wrench (1999), Diurnal variations of 20 GHz and 40 GHz slant path attenuation statistics in southern England, paper presented at National Conference on Antennas and Propagation, Inst. of Electr. Eng., York, U. K.

Wang, J., W. B. Rossow, T. Uttal, and M. Rozendaal (1999), Variability of cloud vertical structure during ASTEX observed from a combination of rawinsonde, radar, ceilometer, and satellite, *Mon. Weather Rev.*, *127*, 2484–2502.

Ware, R., R. Carpenter, J. Güldner, J. Liljegren, T. Nehrkorn, F. Solheim, and F. Vandenberghe (2003), A multichannel radiometric profiler of temperature, humidity, and cloud liquid, *Radio Sci.*, *38*(4), 8079, doi:10.1029/2002RS002856.

Wentz, F. (1997), A well-calibrated ocean algorithm for SSM/I, *J. Geophys. Res.*, *102*, 8703–8718.

Xue, M., K. K. Droegemeier, and V. Wong (2000), The Advanced Regional Prediction System (ARPS)—A multi-scale nonhydrostatic atmospheric simulation model. part I: Model dynamics and verification, *Meteorol. Atmos. Phys.*, *75*, 161–193.

Xue, M., K. K. Droegemeier, V. Wong, A. Shapiro, K. Brewster, F. Carr, D. Weber, Y. Liu, and D. Wang (2001), The Advanced Regional Prediction System (ARPS)—A multi-scale nonhydrostatic atmospheric simulation tool. part II: Model physics and application, *Meteorol. Atmos. Phys.*, *76*, 143–165.

Zhang, G. (2003), Lagrangian study of cloud properties and their relationships to meteorological parameters over the U.S. southern Great Plains, *J. Clim.*, *16*, 2700–2716.

F. S. Marzano, N. Pierdicca, and L. Pulvirenti, Dept. of Electronic Engineering, University La Sapienza of Rome, Rome, I-00184, Italy. (pulvirenti@mail.die.uniroma1.it)